Available online at www.sciencedirect.com
SCIENCE DIRECT®
Journal of Organometallic Chemistry 690 (2005) 2191–2199
Journal of Organometallic Chemistry
www.elsevier.com/locate/jorganchem

Activation of C–H, C–C and C–I bonds by Pd and *cis*-$Pd(CO)_2I_2$. Catalyst–substrate adaptation

Axel Diefenbach [a,1], F. Matthias Bickelhaupt [b,*]

[a] *Fachbereich Chemie der Philipps-Universität Marburg, Hans-Meerwein-Straße, D-35032 Marburg, Germany*
[b] *Afdeling Theoretische Chemie, Scheikundig Laboratorium der Vrije Universiteit, De Boelelaan 1083, NL-1081 HV Amsterdam, The Netherlands*

Received 1 December 2004; accepted 10 February 2005
Available online 19 March 2005

Abstract

We have studied the oxidative addition reactions of methane and ethane C–H, ethane C–C and iodomethane C–I bonds to Pd and *cis*-$Pd(CO)_2I_2$ at the ZORA-BP86/TZ(2)P level of relativistic density functional theory (DFT). Our purpose, besides exploring these particular model reactions, is to understand how the mechanism of bond activation changes as the catalytically active species changes from a simple, uncoordinated metal atom to a metal–ligand coordination complex. For both Pd and *cis*-$Pd(CO)_2I_2$, direct oxidative insertion (OxIn) is the lowest-barrier pathway whereas nucleophilic substitution (S_N2) is highly endothermic, and therefore not competitive. Introducing the ligands, i.e., going from Pd to *cis*-$Pd(CO)_2I_2$, causes a significant increase of the activation and reaction enthalpies for oxidative insertion and takes away the intrinsic preference of Pd for C–I over C–H activation. Obviously, *cis*-$Pd(CO)_2I_2$ is a poor catalyst in terms of activity as well as selectivity for one of the three bonds studied. However, its exploration sheds light on features in the process of catalytic bond activation associated with the increased structural and mechanistic complexity that arises if one goes from a monoatomic model catalysts to a more realistic transition-metal complex. First, in the transition state (TS) for oxidative insertion, the C–X bond to be activated can have, in principle, various different orientations with respect to the square-planar *cis*-$Pd(CO)_2I_2$ complex, e.g., C–X or X–C along an I–Pd–CO axis, or in between two I–Pd–CO axes. Second, at variance to the uncoordinated metal atom, the metal complex may be deformed due to the interaction with the substrate. This leads to a process of mutual adjustment of catalyst and substrate that we designate catalyst–substrate adaptation. The latter can be monitored by the Activation Strain model in which activation energies $\Delta E^{\neq}$ are decomposed into the activation strain $\Delta E^{\neq}_{\text{strain}}$ of and the stabilizing TS interaction $\Delta E^{\neq}_{\text{int}}$ between the reactants in the activated complex: $\Delta E^{\neq} = \Delta E^{\neq}_{\text{strain}} + \Delta E^{\neq}_{\text{int}}$.

Keywords: Activation strain model; Bond activation; Catalyst design; Density functional calculations; Oxidative addition; Palladium

1. Introduction

Oxidative addition and reductive elimination (Eq. (1)) are ubiquitous in homogeneous catalysis [1] and have been intensively studied both experimentally [2–6] and theoretically [6–12].

$$ML_n + R\text{–}X \underset{\text{reductive elimination}}{\overset{\text{oxidative addition}}{\rightleftharpoons}} R\text{–}ML_n\text{–}X \qquad (1)$$

Previously, we have studied the reactions of uncoordinated Pd(0) and $PdCl^-$ toward H–H, C–H, C–C and C–Cl bonds [12]. Palladium was chosen because this metal is widely used in catalysis [2] and because this *atom* has, at variance with, for example, nickel or platinum, a stable closed-shell d^{10} ground state. The latter facilitates the comparison with catalytic Pd(0) or Pd(II) *complexes* the main common characteristic of which, as regards their reactivity, is in general a closed-shell

* Corresponding author. Tel.: +31 20 59 87617; fax: +31 20 59 87629.
E-mail address: FM.Bickelhaupt@few.vu.nl (F.M. Bickelhaupt).
[1] Present address: Sercon GmbH, Germany.

0022-328X/$ - see front matter © 2005 Elsevier B.V. All rights reserved.
doi:10.1016/j.jorganchem.2005.02.013

electronic structure (as opposed to an open-shell or radical behavior). In the present study, we have carried out such a comparison between the reactivity of the Pd atom and that of the *cis*-$Pd(CO)_2I_2$ complex in which palladium is formally Pd(II) with an effective d^8 configuration. Note that *cis*-$Pd(CO)_2I_2$ is isoelectronic with the also square planar complex $[Rh(CO)_2I_2]^-$, one of the catalytically active species that promotes C–I bond activation in the Monsanto acetic acid process [1a,3]. We have investigated the activation by these model catalysts of the archetypal C–H, C–C and C–I bonds by exploring and analyzing the oxidative addition pathways, both via direct oxidative insertion (OxIn) and backside nucleophilic substitution (S_N2), of Pd and *cis*-$Pd(CO)_2I_2$ with CH_4, C_2H_6 and CH_3I (Eqs. 2–5):

$$Pd + CH_4 \rightarrow CH_3 - Pd\text{–}H \tag{2a}$$

$$Pd(CO)_2I_2 + CH_4 \rightarrow CH_3\text{–}[Pd(CO)_2I_2]\text{–}H \tag{2b}$$

$$Pd + C_2H_6 \rightarrow C_2H_5\text{–}Pd\text{–}H \tag{3a}$$

$$Pd(CO)_2I_2 + C_2H_6 \rightarrow C_2H_5\text{–}[Pd(CO)_2I_2]\text{–}H \tag{3b}$$

$$Pd + C_2H_6 \rightarrow CH_3\text{–}Pd\text{–}CH_3 \tag{4a}$$

$$Pd(CO)_2I_2 + C_2H_6 \rightarrow CH_3\text{–}[Pd(CO)_2I_2]\text{–}CH_3 \tag{4b}$$

$$Pd + CH_3I \rightarrow CH_3\text{–}Pd\text{–}I \tag{5a}$$

$$Pd(CO)_2I_2 + CH_3I \rightarrow CH_3\text{–}[Pd(CO)_2I_2]\text{–}I \tag{5b}$$

Note that *cis*-$Pd(CO)_2I_2$ is not a "real-world" catalyst in the sense that, as will be seen later on, it does not speed up and even retards the bond activation processes relative to the uncoordinated Pd atom. However, by exploring the reactivity of the *cis*-$Pd(CO)_2I_2$ model catalyst, one can reveal and learn about interesting features that can occur only in structurally more complex model catalysts that involve ligands coordinated to the transition-metal core. For example, in the TS for oxidative insertion, the C–X bond (X = H, C, I) to be activated can have, in principle, different orientations with respect to the square-planar *cis*-$Pd(CO)_2I_2$ complex, e.g., C–X or X–C along an I–Pd–CO axis, or in between two I–Pd–CO axes. Furthermore, at variance to the uncoordinated metal, the metal complex may be deformed in the TS.

The above-mentioned effects on the competition between the various bond activation processes and mechanisms is interpreted in terms of the Activation Strain model of chemical reactivity originally introduced in the context of elementary organic reactions [8,11,12]. In this model, activation energies $\Delta E^{\neq}$ are decomposed into the activation strain $\Delta E^{\neq}_{\text{strain}}$ of and the stabilizing transition state (TS) interaction $\Delta E^{\neq}_{\text{int}}$ between the reactants in the activated complex: $\Delta E^{\neq} = \Delta E^{\neq}_{\text{strain}} + \Delta E^{\neq}_{\text{int}}$. Recently, in our studies on oxidative addition of H–H and C–X bonds to Pd and $PdCl^-$ [12], we have shown that the activation strain adopts characteristic values for a particular bond and reaction mechanism. The new features encountered in the reactions of the *cis*-$Pd(CO)_2I_2$ complex, in particular, the substantial deformation that the square-planar transition-metal complex may undergo, lead to an extension of the Activation Strain model that is presented in Section 3.2. We show how the concepts of activation strain and TS interaction can be used to categorize and also design catalysts.

The long-term purpose of these efforts is understanding and directing, in a rational manner, the factors that determine the catalytic activity and selectivity of *solution-phase* transition metal *complexes*. However, as pointed out before, the starting point is the investigation of the *intrinsic* reactivity of the transition metal *atom* [8,9,12]. In a second stage, by introducing ligands, it can be precisely assessed how they interfere with the metal electronic structure and why exactly they cause a particular change in the activity and selectivity of the resulting homogeneous catalyst. This modular approach to theoretical homogeneous catalysis, in which the catalyst is assembled step by step to uncover and understand the function of its individual components, has been designated fragment-oriented design of catalysts (FDC) [12]. Recently, we have analyzed the mechanism through which anion assistance influences palladium-catalyzed C–X (and H–H) bond activation by introducing one single chloride anion on Pd(0) [12a,c]. In the present study, we proceed by completely saturating the coordination sphere of the palladium core, which leads to the above-mentioned new features, in particular, a component in the activation strain, $\Delta E^{\neq}_{\text{strain, cat}}$, that stems from the structural deformation of the model catalyst associated with the mutual catalyst–substrate adaptation in the TS of the bond-activation process.

2. Methods

All calculations are based on density functional theory (DFT) [13,14] and have been performed using the Amsterdam density functional (ADF) program [15]. MOs were expanded in a large uncontracted set of Slater-type orbitals (STOs) [15h]. For C, H, O and I, the basis is of triple-ζ quality, augmented with two polarization functions: 2p and 3d for hydrogen, 3d and 4f for carbon and oxygen, and 4d and 4f for iodine. The Pd atom is represented by a triple-ζ type basis set augmented with one set of 5p polarization functions. The core shells of carbon (1s), oxygen (1s), iodine (1s2s2p3s3p3d4s4p) and palladium (1s2s2p3s3p3d) were treated by the frozen-core approximation [15b]. An auxiliary set of s, p, d, f and g STOs was used to fit the

molecular density and to represent the Coulomb and exchange potentials accurately in each SCF cycle [15i].

Geometries and energies were calculated using the generalized gradient approximation (GGA). Exchange is described by Slater's Xα potential [15j], corrected by the nonlocal exchange potential of Becke [15k,l]. Correlation is treated in the Vosko–Wilk–Nusair (VWN) parameterization [15m] using formula V, corrected for nonlocal effects due to Perdew [15n]. Relativistic effects were taken into account by the zeroth-order regular approximation (ZORA) [16].

All energy minima and transition state [15r] structures were verified by frequency calculations [15q]: for minima all normal modes have real frequencies, transition states have one normal mode with an imaginary frequency. The character of the normal mode associated with the imaginary frequency was analyzed to ensure that the correct transition state was found.

Bond enthalpies at 298.15 K and 1 atmosphere (ΔH_{298}) were calculated from 0 K electronic bond energies (ΔE) according to Eq. (6), assuming an ideal gas [17],

$$\Delta H_{298} = \Delta E + \Delta E_{\mathrm{trans},298} + \Delta E_{\mathrm{rot},298} + \Delta E_{\mathrm{vib},0} + \Delta(\Delta E_{\mathrm{vib},0})_{298} + \Delta(pV). \quad (6)$$

Here, $\Delta E_{\mathrm{trans},298}$, $\Delta E_{\mathrm{rot},298}$ and $\Delta E_{\mathrm{vib},0}$ are the differences between products and reactants in translational, rotational and zero point vibrational energy, respectively; $\Delta(\Delta E_{\mathrm{vib}})_{298}$ is the change in the vibrational energy difference as one goes from 0 to 298.15 K. The vibrational energy corrections are based on our frequency calculations. The molar work term $\Delta(pV)$ is $(\Delta n)RT$; $\Delta n = -1$ for two reactants (e.g., [Pd] and CH_3X) combining to one species. Thermal corrections for the electronic energy are neglected.

3. Results and discussion

3.1. Reaction profiles and geometries

In this section, we discuss the potential energy surfaces (PES) of the various oxidative insertion and S_N2 reactions as well as the geometries of the transition states of the various reactions. The results are summarized in Figs. 1 and 2 (geometries) and Tables 1 (thermochemistry) and 2 (activation strain analyses).

First, the straight S_N2 reactions are examined. In line with earlier work [12b], they are highly endothermic and occur without reverse barrier for all model reactions

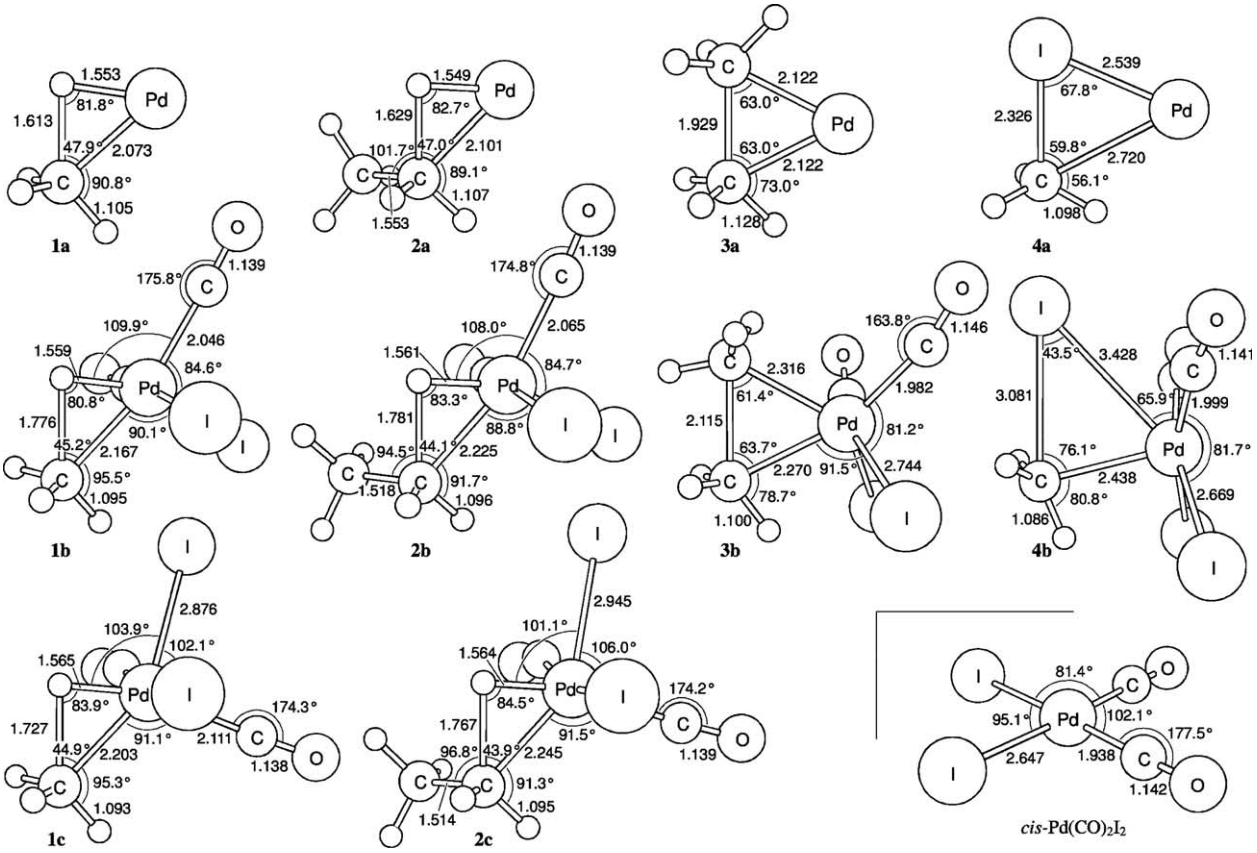

Fig. 1. Geometries (in Å, °) at ZORA-BP86/TZ(2)P of the transition states of direct oxidative insertion reactions of Pd and *cis*-$Pd(CO)_2I_2$ into the methane and ethane C–H, ethane C–C, and iodomethane C–I bonds as well as the equilibrium geometry of *cis*-$Pd(CO)_2I_2$ (see also Fig. 2).

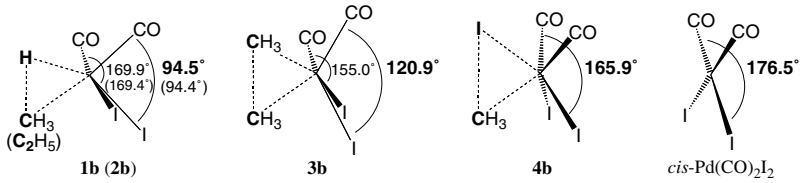

Fig. 2. I–Pd–CO bending angles (in °) in the transition states **1b**–**4b** (see also Fig. 1).

Table 1
Reaction profiles at ZORA-BP86/TZ(2P) for the oxidative insertion of Pd and $Pd(CO)_2I_2$ into the C–H, C–C and C–I bonds of CH_4, C_2H_6 and CH_3I, respectively

Activated bond	Reactants	Reactant complex	Transition state	Product
Direct oxidative insertion				
C–H	Pd + CH_4	−11.4	−5.0	−9.7
	$Pd(CO)_2I_2$ + CH_4[a]	–	48.9	45.1
	$Pd(CO)_2I_2$ + CH_4[b]	–	49.3	44.6
	Pd + C_2H_6	−11.6	−4.1	−11.6[c]
	$Pd(CO)_2I_2$ + C_2H_6[d]	–	47.6	42.7
	$Pd(CO)_2I_2$ + C_2H_6[e]	–	47.8	42.1
C–C	Pd + C_2H_6	−11.6	9.6	−14.1
	$Pd(CO)_2I_2$ + C_2H_6	–	70.9	46.7
C–I	Pd + CH_3I	−23.2	−14.9	−44.0
	$Pd(CO)_2I_2$ + CH_3I	0.2	48.8	20.9
S_N2 Reaction				
C–H	Pd + CH_4	−11.4	–[f]	228.7[g]
	$Pd(CO)_2I_2$ + CH_4	–	–[f]	259.7[g]
C–C	Pd + C_2H_6	−11.6	–[f]	228.6[g]
	$Pd(CO)_2I_2$ + C_2H_6	–	–[f]	259.6[g]
C–I	Pd + CH_3I	–	–[f]	127.0[g]
	$Pd(CO)_2I_2$ + CH_3I	0.2	–[f]	158.6[g]

298 K enthalpies (in kcal/mol) relative to free reactants.
[a] Orientation of catalyst corresponds to structure **1b**, Fig. 1. Chart 1: **O-2**.
[b] Orientation of catalyst corresponds to structure **1c,** Fig. 1. Chart 1: **O-4.**
[c] Primary product of insertion. Rearrangement via second TS (−11.0 kcal/mol) to final product (−12.0 kcal/mol).
[d] Orientation of catalyst corresponds to structure **2b**, Fig. 1. Chart 1: **O-2**.
[e] Orientation of catalyst corresponds to structure **2c**, Fig. 1. Chart 1: **O-4**.
[f] No reverse activation barrier.
[g] Dissociated products of straight S_N2 reaction.

studied. This can be ascribed to charge separation that occurs in the product $PdCH_3^+ + X^-$ and $Pd(CO)_2I_2(CH_3)^+ + X^-$, with X = H, CH_3 and I. In the case of Pd + CH_4, for example, the reaction is endothermic by 228.7 kcal/mol. The endothermicity further increases for all reactions by some 30 kcal/mol if one goes from Pd to the model complex *cis*-$Pd(CO)_2I_2$.

The direct oxidative insertion (OxIn) reactions are much less endothermic; for Pd, they are even exothermic. Each of the reactions involving the uncoordinated Pd atom proceeds first via a reactant complex before the transition state towards the insertion product is encountered. At variance to this, no stable reactant complexes preceding the TS could be identified in the corresponding reactions with *cis*-$Pd(CO)_2I_2$. May be the most striking change if one goes from the Pd- to the *cis*-$Pd(CO)_2I_2$-induced bond activation reactions is the enormous destabilization by 52–64 kcal/mol of transition states and products (see Table 1). For example, the activation energy for oxidative addition of the C–C and C–I bonds increases from +9.6 and −14.9 kcal/mol, respectively, in the case of Pd to +70.9 and +48.8 kcal/mol in the case of *cis*-$Pd(CO)_2I_2$.

Another essential difference between the situation for the uncoordinated Pd atom and *cis*-$Pd(CO)_2I_2$ is that, in the latter, the activated bond can in principle adopt several orientations with respect to the model catalyst. This is illustrated in Chart 1, which shows a number of basic orientations. Of course, also intermediate situations, say, in between **O-1** and **O-2** are conceivable. The *cis*-$Pd(CO)_2I_2$-induced C–H activation in both, CH_4 and C_2H_6, is indeed found to proceed via two distinct transition states, namely, **1b** and **1c** in the case of CH_4 and **2b** and **2c** in the case of C_2H_6 (see Fig. 1). They correspond to orientations that closely resemble **O-2** and **O-4**, respectively (i.e., C–H pointing along I–Pd–CO axis), and are very close in energy, ca. 48–49 kcal/mol above the separate reactants. On the other hand, only one TS could be determined for *cis*-$Pd(CO)_2I_2$-induced activation of either C–C or C–I, as mentioned already above: for C–C the TS (at 70.9 kcal/mol) corresponds to an orientation in between **O-1** and **O-2** and, for C–I, the TS (at 48.8 kcal/mol) has an orientation close to **O-1** (see Table 1 and Fig. 1).

The destabilization of transition states and products in the reactions of *cis*-$Pd(CO)_2I_2$ compared to those of Pd is not uniform. This causes a change in the order of relative TS stabilities from C–I < C–H < C–C for Pd to C–H ≈ C–I ≪ C–C for *cis*-$Pd(CO)_2I_2$, that is, from a situation with a clear preference for C–I activation to a situation in which C–H and C–I activation have essentially the same reaction barrier [18]. Thus, in addition to making the model catalyst inactive, the introduction of two CO ligands and the oxidative addition of iodine to palladium take away its (in principle) selectivity for the C–I bond without returning selectivity for another bond. Obviously, *cis*-$Pd(CO)_2I_2$ is a poor catalyst. The activity may

Table 2
Analysis of the activation energies (in kcal/mol) for Pd and *cis*-$Pd(CO)_2I_2$ induced activation of the indicated bonds in CH_4, C_2H_6 and CH_3I through direct oxidative insertion in terms of the activation strain model

Catalyst	No.	Activation barrier, $\Delta E^{\neq}$	TS interaction, $\Delta E^{\neq}_{int}$	Activation strain, $\Delta E^{\neq}_{strain}$	Catalyst strain, $\Delta E^{\neq}_{strain,cat}$	Substrate strain, $\Delta E^{\neq}_{strain,sub}$
C–H bond activation in CH_4						
Pd	**1a**	−1.6	−55.1	53.5	–	53.5
$Pd(CO)_2I_2$	**1b**	50.5	−54.7	105.2	34.9	70.3
$Pd(CO)_2I_2$	**1c**	51.0	−48.5	99.5	33.6	65.9
C–H bond activation in C_2H_6						
Pd	**2a**	−0.7	−55.4	54.7	–	54.7
$Pd(CO)_2I_2$	**2b**	49.7	−53.0	102.7	35.0	67.7
$Pd(CO)_2I_2$	**2c**	49.8	−50.9	100.7	34.4	66.3
C–C bond activation in C_2H_6						
Pd	**3a**	12.6	−26.8	39.4	–	39.4
$Pd(CO)_2I_2$	**3b**	72.6	−18.8	91.4	31.9	59.5
C–I bond activation in CH_3I						
Pd	**4a**	−15.2	−19.3	4.1	–	4.1
$Pd(CO)_2I_2$	**4b**	49.7	−9.5	59.2	4.0	55.2

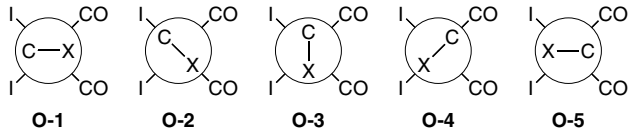

Chart 1. Relative orientations of catalytic metal complex and C–X bond.

again be substantially improved by introducing a negative charge, either through adding an additional anionic ligand, e.g., I^-, or by going from Pd (group 10) to Rh or Ir (group 9) [1a,3,7d,12a,c]. This is consistent with the experimental observations that the anionic $[Rh(CO)_2I_2]^-$ complex does induce iodomethane C–I activation and that this process is enhanced by coordination of an additional iodide ligand in $[Rh(CO)_2I_3]^{2-}$ [1a,3]. Note however that introducing a fifth ligand, such as in $Pd(CO)_2I_3^-$, will disfavor the OxIn pathway as this would lead to a sterically over-crowded seven-coordinate complex $Pd(CO)_2I_3(CH_3)(X)^-$.

As can be seen in Fig. 1, the C–X bond is significantly more expanded in the transition states of the *cis*-$Pd(CO)_2I_2$-induced oxidative insertion reactions than in the Pd-induced ones. In the former, the activated bond is expanded by ca. 60% (C–H in methane and ethane), 38% (C–C) and 42% (C–I) whereas, in the latter, it is elongated only ca. 48% (C–H in methane and ethane), 26% (C–C) and 7% (C–I). Furthermore, activation of the C–H bond via **O-2** orientation (i.e., along the I–Pd–CO axis with hydrogen pointing toward the CO ligand, see Chart 1) goes with slightly more C–H bond elongation than via **O-4** orientation (i.e., along the I–Pd–CO axis with hydrogen pointing toward the I^- ligand). The C–H bond of CH_4, for example, is stretched by 0.517 Å (47%) and amounts to 1.613 Å in the TS when activated by Pd. In the case of *cis*-$Pd(CO)_2I_2$, this C–H bond is stretched by 0.680 Å (62%) and amounts to 1.776 Å in transition state **1b** with **O-2** orientation.

The more product-like structure of the transition states involving *cis*-$Pd(CO)_2I_2$ in combination with the increased endothermicity (see Table 1) is reminiscent of the Hammond postulate. This holds also for the trends along C–H, C–C and C–I, for which the extent of deformation decreases (i.e., the TS becomes more educt-like) as the reaction becomes more exothermic (Pd) or less endothermic (*cis*-$Pd(CO)_2I_2$; see Fig. 1 and Table 1). The trend of decreasing deformation in the TS along C–H, C–C and C–I is obvious for the Pd-induced reactions for which we can simply inspect the percentage wise bond elongation in the transition state,

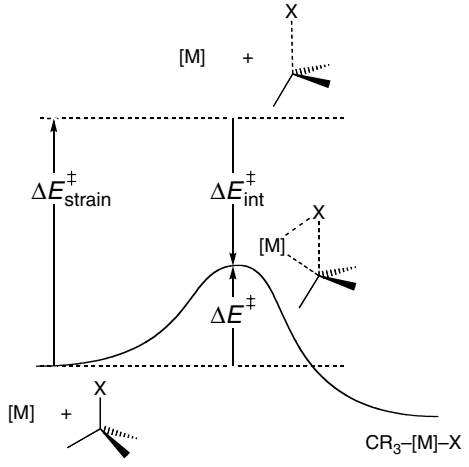

Fig. 3. Illustration of the Activation Strain model in case of C–X bond activation by a transition metal system [M]. The activation energy $\Delta E^{\neq}$ is decomposed into the activation strain $\Delta E^{\neq}_{strain}$ of and the stabilizing TS interaction $\Delta E^{\neq}_{int}$ between the reactants in the transition state. The activation strain $\Delta E^{\neq}_{strain}$ can be divided into the contributions from substrate, $\Delta E^{\neq}_{strain,sub}$, and catalyst, $\Delta E^{\neq}_{strain,cat}$.

which indeed decreases (see above). In the case of the *cis*-$Pd(CO)_2I_2$-induced reactions this is somewhat less obvious at first sight. Here, the percentage-wise elongation of the C–X bond first decreases from C–H (ca. 60%) to C–C (38%) but thereafter it increases again if one goes to C–I (42%). However, here we also have to take into account the extent to which the *cis*-$Pd(CO)_2I_2$ model catalyst is deformed in the transition state. The key geometry parameters, here, are the I–Pd–CO bending angles. The values of the latter for transition states **1b**–**4b** are shown in Fig. 2. As can be seen here, the extent to which the iodide and carbon monoxide ligand bend away from the approaching substrate decreases steeply along C–H, C–C and C–I with I–Pd–CO angles of 95°, 121° and 166°, respectively. For comparison, in the undeformed *cis*-$Pd(CO)_2I_2$ complex (planar, C_{2v} point group symmetry), the I–Pd–CO angle amounts to 177°. Thus, overall, the extent of deformation decreases (i.e., the TS becomes more educt-like) as the reaction becomes less endothermic. Later on, in Section 3.3, we will come back to this issue.

3.2. The activation strain model

3.2.1. Activation strain and TS interaction

To gain insight into how introduction of ligands affects the activation barriers of the different oxidative insertion reactions, i.e., insight into how this effect depends on the nature of the concomitant geometrical deformation and electronic structure of catalyst and substrate, they were analyzed using the Activation Strain model of chemical reactivity [8,11,12]. In this model, the activation energy $\Delta E^{\neq}$ is decomposed into the activation strain $\Delta E^{\neq}_{\text{strain}}$ and the transition state (TS) interaction $\Delta E^{\neq}_{\text{int}}$ (see Eq. (7) and Fig. 3):

$$\Delta E^{\neq} = \Delta E^{\neq}_{\text{strain}} + \Delta E^{\neq}_{\text{int}}. \tag{7}$$

The activation strain $\Delta E^{\neq}_{\text{strain}}$ is the strain energy associated with deforming the reactants from their equilibrium geometry to the geometry they acquire in the activated complex (Fig. 3). The TS interaction $\Delta E^{\neq}_{\text{int}}$ is the actual interaction energy between the deformed reactants in the transition state. In the present study, one of the reactants is either the neutral, uncoordinated Pd-d^{10} atom or the model complex *cis*-$Pd(CO)_2I_2$ and the other reactant is one of the substrates CH_4, C_2H_6, and CH_3I.

3.2.2. Catalyst–substrate adaptation

The structurally very simple mono- and diatomic model catalysts that we have studied previously, contribute only marginally ($PdCl^-$) or not at all (Pd) to the activation strain $\Delta E^{\neq}_{\text{strain}}$, which then predominantly or completely originates from the substrate in which the C–X bond must naturally expand during the process of bond activation [12]. This changes in the case of the model catalyst *cis*-$Pd(CO)_2I_2$ in which the active metal core is surrounded by four ligands. In the course of the C–X oxidative addition, these ligands must bend back to avoid steric repulsion with and generate space for the approaching substrate that, eventually, dissociates into two new ligands (CH_3^- and X^-), resulting in hexacoordinate [Pd-$d^6$$(CO)_2I_2(CH_3)(X)$]. Thus, introducing more than one ligand into the catalytically active transition metal system brings into play the phenomenon of ligand reorganization as an additional important factor that affects the activation strain. This phenomenon can be conceived as a mutual adaptation of catalyst and substrate as they approach toward the transition state. To monitor the process of catalyst–substrate adaptation, the activation strain is decomposed into a part belonging to the catalyst, $\Delta E^{\neq}_{\text{strain,cat}}$, and a part representing the substrate, $\Delta E^{\neq}_{\text{strain,sub}}$, see Eq. (8).

$$\Delta E^{\neq} = \Delta E^{\neq}_{\text{strain, cat}} + \Delta E^{\neq}_{\text{strain, sub}} + \Delta E^{\neq}_{\text{int}} \tag{8}$$

3.3. Analysis of the reaction barriers for bond activation

The results of the Activation Strain analysis are collected in Table 2. Introducing the ligands, i.e., going from Pd to *cis*-$Pd(CO)_2I_2$, causes, as mentioned above, an increase of the activation and reaction enthalpies for all bonds and for both types of mechanisms, i.e., direct oxidative insertion (OxIn) and the S_N2 pathway. The latter pathway is under all conditions completely inaccessible because of the energetically immensely unfavorable charge separation in the products. Here, we focus on understanding the effect of introducing ligands in case of direct oxidative insertion (OxIn) into the C–H, C–C and C–I bonds.

The activation energies $\Delta E^{\neq}$of both, the Pd- and *cis*-$Pd(CO)_2I_2$-induced bond activation reactions, are highest for C–C and decrease if one goes to C–H or C–I, but those of the latter, the *cis*-$Pd(CO)_2I_2$-induced reaction, are 52–65 kcal/mol higher (see Tables 1 and 2). The main source of this rise in activation energies is the activation strain $\Delta E^{\neq}_{\text{strain}}$, which increases by 46–55 kcal/mol (see Table 2). Note that the TS interaction $\Delta E^{\neq}_{\text{int}}$ also contributes to the rise in activation energy, although much less, with a weakening of 0.4–9.8 kcal/mol. The trend in activation strain reflects the larger geometrical deformations, i.e., the more product-like structure, in the *cis*-$Pd(CO)_2I_2$-induced transition states discussed in Section 3.1 (see also Figs. 1 and 2). For example, the percentage-wise bond elongation in the TS and the activation strain for C–C bond activation goes from +26% and 39.4 kcal/mol for Pd to +38% and 91.4 kcal/mol for *cis*-$Pd(CO)_2I_2$.

As already pointed out above, the activation strain is not only due to the elongation of the C–X bond (and to

other deformations associated with the substrate, such as tilting of methyl groups) but also to ligand reorganization in the model catalyst, in particular, the back-bending of ligands as the CH_3X substrate approaches. The catalyst–substrate adaptation is in fact a complex process in which both, catalyst and substrate, mutually influence and structurally react to each other. A full understanding of this process requires an exploration and detailed analysis of the interplay of the catalyst–substrate interaction $\Delta E_{\text{int}}(\zeta)$, the strain in the substrate $\Delta E_{\text{strain, sub}}(\zeta)$ and the strain in the catalyst $\Delta E_{\text{strain, cat}}(\zeta)$ as a function of the reaction coordinate ζ, which is beyond the scope of the present investigation. Here, we focus on the stationary points along the reaction coordinate, which already leads to interesting observations. First, the increase in activation strain from Pd to *cis*-$Pd(CO)_2I_2$ is indeed caused by both, an increase in the substrate component $\Delta E^{\neq}_{\text{strain,sub}}$ and the addition of the catalyst component $\Delta E^{\neq}_{\text{strain,cat}}$. More importantly, the relative distribution of strain between catalyst and substrate is not constant and it appears to be correlated with the strength ΔH_{bond} of the activated bond, which decreases from 99 kcal/mol for C–H to 83 kcal/mol for C–C to 51 kcal/mol for C–I [19]. Note that, in parallel with this trend, the overall activation strain decreases in the same order along C–H, C–C and C–I, namely, from ca. 54 to 39 to 4 kcal/mol for Pd-induced reactions and from 66–70 to 60 to 55 kcal/mol for the *cis*-$Pd(CO)_2I_2$-induced reactions. This is in line with earlier work on oxidative insertion of Pd and $PdCl^-$ into H–H, C–H, C–C and C–Cl bonds [12]. Note however also that the contribution of $\Delta E^{\neq}_{\text{strain,cat}}$ also decreases from ca. 34% for C–H and C–C to 7% for C–I or, in terms of absolute values, from ca. 34 to 32 to only 4 kcal/mol for C–H, C–C and C–I. This correlates again nicely with the extent of geometrical deformation of the *cis*-$Pd(CO)_2I_2$ model catalyst in the TS, as pointed out in Section 3.1 (see Fig. 2). Thus, a simple and physically plausible picture emerges: a softer C–X bond will absorb a larger fraction of the strain associated with the mutual approach of substrate and catalyst toward the TS.

The above analyses also shed light from a different perspective on the role of the bite angle in catalytic transition metal complexes involving bridged diphosphine ligands. The bite angle is generally discussed in terms of its consequences: (i) for the frontier-orbital electronic structure of the catalyst, and (ii) for the steric demand of the ligand (and thus the catalyst), both of which affect the catalyst–substrate interaction [20]. The present study emphasizes that fixing the bite angle also assist the reaction by taking away the catalyst's component of the activation strain from the activation energy. This is because the strain associated with bending the ligands towards the natural (or optimal or desired) angle in the TS is now built-in, from the outset, into the catalytically active transition-metal complex. For example, by fixing the I–Pd–CO angle to ca. 95° in the methane C–H activation through TS **1b** (see Figs. 1 and 2), we could reduce the activation energy approximately by 35 kcal/mol, i.e., the value of $\Delta E^{\neq}_{\text{strain,cat}}$ (see Table 2). In the case of our present model catalyst, fixing the bite angle is of course a fictitious undertaking, as the ligands, CO and I, do not offer the possibility of introducing a bridge. However, we feel that the idea of "taking away" $\Delta E^{\neq}_{\text{strain,cat}}$ by building the catalyst–substrate adaptation (and thus the associated activation strain) into the catalyst, can be easily transferred to and assists a more rational design of catalysts involving bidentate ligands with a tunable bite angle. Indeed, this expectation is confirmed by the preliminary results for oxidative insertion of $Pd(PH_3)_2$ into the methane C–H bond. Compared to the corresponding process for uncoordinated Pd, the activation energy for the diphosphine complex is upraised by ca. 28 kcal/mol. This increase in the barrier stems nearly entirely from the increased activation strain associated with bending back the phosphine ligands in the transition state, while the TS interaction is constant within a few tenths of a kcal/mol.

4. Conclusions

Introducing ligands, i.e., going from uncoordinated Pd^0 to the *cis*-$Pd^{II}(CO)_2I_2$, causes a significant increase of the activation and reaction enthalpies (up to 65 kcal/mol computed at ZORA-BP86/TZ(2)P) for oxidative insertion (OxIn) into C–H, C–I and C–C bonds and takes away the intrinsic preference of Pd for C–I over C–H activation. The activation barriers for *cis*-$Pd^{II}(CO)_2I_2$ increase in the order C–H (48–49 kcal/mol) $\approx$ C–I (49 kcal/mol) $\ll$ C–C (71 kcal/mol).

The main source of the rise in activation energies for *cis*-$Pd^{II}(CO)_2I_2$ is the activation strain $\Delta E^{\neq}_{\text{strain}}$, the increase in energy associated with the geometrical deformation of both substrate and catalyst as they approach toward the transition state. The activation strain $\Delta E^{\neq}_{\text{strain}}$ correlates with the strength ΔH_{bond} of the activated C–X bond: both decrease along C–H, C–C and C–I. Interestingly, also the internal distribution of strain between catalyst and substrate correlates with the C–X bond strength: the softer the C–X bond the larger the fraction of activation strain it absorbs. Thus, the substrate component of $\Delta E^{\neq}_{\text{strain}}$ and the C–X bond expansion in the TS increases while the catalyst component decreases along C–H, C–C and C–I.

Finally, we have argued that the role of a fixed bite angle in transition metal complexes is not only to obtain an optimal catalyst electronic structure and steric demand but also to build-in the catalyst-component $\Delta E^{\neq}_{\text{strain,cat}}$ of the activation strain into the catalyst itself. This idea can be used in the rational design of catalysts

to take away $\Delta E^{\neq}_{\text{strain,cat}}$ and accordingly lower the barrier of a particular reaction.

Acknowledgements

We thank the Fonds der Chemischen Industrie (FCI) for a doctoral stipendium for A.D., the Netherlands Organization for Scientific Research (NWO-CW) for financial support, and G. Th. de Jong for helpful discussions.

References

[1] (a) J.P. Collman, L.S. Hegedus, J.R. Norton, R.G. Finke, Principles and applications of organotransition metal chemistry, University Science Books, Mill Valley, CA, 1987;
(b) Ch. Elschenbroich, A. Salzer, Organometallics. A Concise Introduction, second ed., VCH, Weinheim, Germany, 1992;
(c) C. Amatore, A. Jutand, Acc. Chem. Res. 33 (2000) 314;
(d) T.-Y. Luh, M.-k. Leung, K.-T. Wong, Chem. Rev. 100 (2000) 3187;
(e) R.H. Crabtree, Chem. Rev. 95 (1995) 987;
(f) V.V. Grushin, H. Alper, Chem. Rev. 94 (1994) 1047.

[2] (a) P. Espinet, A.M. Echavarren, Angew. Chem. 116 (2004) 4808;
(b) J.-L. Malleron, J.-C. Fiaud, J.-Y. Legros, Handbook of palladium catalyzed organic reactions, Academic Press, 1997;
(c) R. Cornils, W.A. HerrmannApplied Homogenous Catalysis with Organometallic Compounds, vol. 1, VCH, Weinheim, 1996, p. 394.

[3] (a) C.E. Hickey, P.M. Maitlis, J. Chem. Soc., Chem. Commun. (1984) 1609;
(b) D. Forster, Adv. Organomet. Chem. 17 (1979) 255;
(c) D. Forster, J. Am. Chem. Soc. 97 (1975) 951.

[4] (a) K. Eller, H. Schwarz, Chem. Rev. 91 (1991) 1121;
(b) P.B. Armentrout, J.L. Beauchamp, Acc. Chem. Res. 22 (1989) 315.

[5] (a) Experimental studies on reactions of neutral metal atoms in the gas phase: Y. Wen, M. Porembski, T.A. Ferrett, J.C. Weisshaar, J. Phys. Chem. A 102 (1998) 8362;
(b) Y. Wen, A. Yethiraj, J.C. Weisshaar, J. Chem. Phys. 106 (1997) 5509;
(c) J.J. Carroll, J.C. Weisshaar, J. Phys. Chem. 100 (1996) 12355;
(d) G.V. Chertihin, L. Andrews, J. Am. Chem. Soc. 116 (1994) 8322;
(e) J.J. Carroll, K.L. Haug, J.C. Weisshaar, J. Am. Chem. Soc. 115 (1993) 6962;
(f) J.J. Carroll, J.C. Weisshaar, J. Am. Chem. Soc. 115 (1993) 800;
(g) D. Ritter, J.J. Carroll, J.C. Weisshaar, J. Phys. Chem. 96 (1992) 10636;
(h) S.A. Mitchell, P.A. Hackett, J. Chem. Phys. 93 (1990) 7822;
(i) D. Ritter, J.C. Weisshaar, J. Am. Chem. Soc. 112 (1990) 6425;
(j) P. Fayet, A. Kaldor, D.M. Cox, J. Chem. Phys. 92 (1990) 254.

[6] (a) Combined experimental and theoretical studies: A. Haynes, P.M. Maitlis, G.E. Morris, G.J. Sunley, H. Adams, P.W. Badger, C.M. Bowers, D.B. Cook, P.I.P. Elliot, T. Ghaffar, H. Green, T.R. Griffin, M. Payne, J.M. Pearson, M.J. Taylor, P.W. Vickers, R.J. Watt, J. Am. Chem. Soc. 126 (2004) 2847;
(b) M. Porembski, J.C. Weisshaar, J. Phys. Chem. A 104 (2000) 1524;
(c) J.J. Carroll, K.L. Haug, J.C. Weisshaar, M.R.A. Blomberg, P.E.M. Siegbahn, M. Svensson, J. Phys. Chem. 99 (1995) 13955;
(d) J.J. Carroll, J.C. Weisshaar, P.E.M. Siegbahn, A.M.C. Wittborn, M.R.A. Blomberg, J. Phys. Chem. 99 (1995) 14388;
(e) S. Mitchell, M.A. Blitz, P.E.M. Siegbahn, M. Svenson, J. Chem. Phys. 100 (1994) 423;
(f) J.C. Weisshaar, Acc. Chem. Res. 26 (1993) 213.

[7] (a) Theoretical studies on reactions of metal complexes: H.M. Senn, T. Ziegler, Organometallics 23 (2004) 2980;
(b) A. Dedieu, Chem. Rev. 100 (2000) 543;
(c) M. Torrent, M. Solà, G. Frenking, Chem. Rev. 100 (2000) 439;
(d) T.R. Griffin, D.B. Cook, A. Haynes, J.M. Pearson, D. Monti, G.E. Morris, J. Am. Chem. Soc. 118 (1996) 3029;
(e) G. Aullón, S. Alvarez, Inorg. Chem. 35 (1996) 3137;
(f) T. Ziegler, Chem. Rev. 91 (1991) 651;
(g) N. Koga, K. Morokuma, Chem. Rev. 91 (1991) 823;
(h) F.M. Bickelhaupt, E.J. Baerends, W. Ravenek, Inorg. Chem. 29 (1990) 350.

[8] F.M. Bickelhaupt, J. Comput. Chem. 20 (1999) 114.

[9] F.M. Bickelhaupt, T. Ziegler, P. von Ragué Schleyer, Organometallics 14 (1995) 2288.

[10] (a) Theoretical studies on reactions of neutral metal atoms: F. Maseras, A. Lledós, E. Clot, O. Eisenstein, Chem. Rev. 100 (2000) 601;
(b) Q. Cui, D.G. Musaev, K. Morokuma, J. Chem. Phys. 108 (1998) 8418;
(c) A.M.C. Wittborn, M. Costas, M.R.A. Blomberg, P.E.M. Siegbahn, J. Chem. Phys. 107 (1997) 4318;
(d) P.E.M. Siegbahn, J. Am. Chem. Soc. 116 (1994) 7722;
(e) P.E.M. Siegbahn, Organometallics 13 (1994) 2833;
(f) J.K. Perry, G. Ohanessian, W.A. Goddard III, Organometallics 13 (1994) 1870;
(g) M.R.A. Blomberg, P.E.M. Siegbahn, M. Svensson, Inorg. Chem. 32 (1993) 4218;
(h) P.E.M. Siegbahn, M.R.A. Blomberg, M. Svensson, J. Phys. Chem. 97 (1993) 2564;
(i) P.E.M. Siegbahn, M.R.A. Blomberg, M. Svensson, J. Am. Chem. Soc. 115 (1993) 1952.

[11] A. Diefenbach, F.M. Bickelhaupt, J. Chem. Phys. 115 (2001) 4030.

[12] (a) A. Diefenbach, G.Th. de Jong, F.M. Bickelhaupt, Mol. Phys. 103 (2005) in press;
(b) A. Diefenbach, F.M. Bickelhaupt, J. Phys. Chem. A 108 (2004) 8460;
(c) A. Diefenbach, G.Th. de Jong, F.M. Bickelhaupt, J. Chem. Theory Comput. 1 (2005) in press.

[13] (a) R.M. Dreizler, E.K.U. Gross, Density Functional Theory. An Approach to the Quantum Many-body Problem, Springer, Berlin, 1990;
(b) R.G. Parr, W. Yang, Density-functional theory of atoms and molecules, Oxford University Press, New York, 1989.

[14] (a) Kohn–Sham MO model in DFT F.M. Bickelhaupt, E.J. Baerends, in: K.B. Lipkowitz, D.B. Boyd (Eds.), Reviews in Computational Chemistry, vol. 15, Wiley-VCH, New York, 2000 (Chapter 1);
(b) E.J. Baerends, O.V. Gritsenko, J. Phys. Chem. A 101 (1997) 5383.

[15] (a) Amsterdam density functional (ADF) program: G. te Velde, F.M. Bickelhaupt, E.J. Baerends, S.J.A. van Gisbergen, C. Fonseca Guerra, J.G. Snijders, T. Ziegler, J. Comput. Chem. 22 (2001) 931;
(b) E.J. Baerends, D.E. Ellis, P. Ros, Chem. Phys. 2 (1973) 41;
(c) E.J. Baerends, P. Ros, Chem. Phys. 8 (1975) 412;
(d) E.J. Baerends, P. Ros, Int. J. Quantum Chem., Quantum Chem. Symp. S12 (1978) 169;
(e) C. Fonseca Guerra, J.G. Snijders, G. te Velde, E. Baerends, J. Theor. Chem. Acc. 99 (1998) 391;

(f) P.M. Boerrigter, G. te Velde, E. Baerends, J. Quantum, J. Int. Chem. 33 (1988) 87;
(g) G. te Velde, E.J. Baerends, J. Comp. Phys. 99 (1992) 84;
(h) J.G. Snijders, E.J. Baerends, P. Vernooijs, At. Nucl. Data Tables 26 (1982) 483;
(i) J. Krijn, E.J. Baerends, Fit-functions in the HFS-method, Internal report (in Dutch), Vrije Universiteit, Amsterdam, 1984;
(j) J.C. SlaterQuantum Theory of Molecules and Solids, vol. 4, McGraw-Hill, New York, 1974;
(k) A.D. Becke, J. Chem. Phys. 84 (1986) 4524;
(l) A. Becke, Phys. Rev. A 38 (1988) 3098;
(m) S.H. Vosko, L. Wilk, M. Nusair, Can. J. Phys. 58 (1980) 1200;
(n) J.P. Perdew, Phys. Rev. B 33 (1986) 8822, Erratum: Phys. Rev. B 34 (1986) 7406;
(o) L. Fan, T. Ziegler, J. Chem. Phys. 94 (1991) 6057;
(p) L. Versluis, T. Ziegler, J. Chem. Phys. 88 (1988) 322;
(q) L. Fan, T. Ziegler, J. Chem. Phys. 92 (1990) 3645;
(r) L. Fan, L. Versluis, T. Ziegler, E.J. Baerends, W. Ravenek, Int. J. Quantum. Chem., Quantum. Chem. Symp. S22 (1988) 173.

[16] (a) C. Chang, M. Pelissier, P. Durand, Phys. Scr. 34 (1986) 394;
(b) E. van Lenthe, E.J. Baerends, J.G. Snijders, J. Chem. Phys. 99 (1993) 4597;
(c) E. van Lenthe, E.J. Baerends, J.G. Snijders, J. Chem. Phys. 101 (1994) 9783;
(d) E. van Lenthe, R. van Leeuwen, E.J. Baerends, J.G. Snijders, Int. J. Quantum Chem. 57 (1996) 281.

[17] P.W. Atkins, Physical Chemistry, Oxford University Press, Oxford, 1998.

[18] This is a comparison between the Pd-induced activation of the C–H bond in methane and the C–I bond in iodomethane. Preliminary computations for the corresponding reactions with chlorine instead of iodine suggest that the same conclusions hold if we would compare Pd-induced activation of C–H and C–I both in iodomethane, i.e., CH_2I–H versus CH_3–I. Thus, the computed activation energies for OxIn of Pd into a C–H bond of methane and chloromethane are equal and both amount to −1.6 kcal/mol. On the other hand, the activation energy for OxIn of Pd into the C–Cl bond of chloromethane is nearly 3 kcal/mol lower and amounts to −4.3 kcal/mol.

[19] A.F. Holleman, N. Wiberg, Lehrbuch Der Anorganischen Chemie, de Gruyter, Berlin, 1985.

[20] (a) See, for example: P.C.J. Kamer, P.W.N.M. van Leeuwen, J.N.H. Reek, Acc. Chem. Res. 34 (2001) 895;
(b) L.A. van der Veen, P.H. Keeven, G.C. Schoemaker, J.N.H. Reek, P.C.J. Kamer, P.W.N.M. van Leeuwen, M. Lutz, A.L. Spek, Organometallics 19 (2000) 872;
(c) P.W.N.M. van Leeuwen, P.C.J. Kamer, J.N.H. Reek, P. Dierkes, Chem. Rev. 100 (2000) 2741;
(d) D.L. Thorn, R. Hoffmann, J. Am. Chem. Soc. 100 (1978) 2079.